

# Harmonic generation of noble-gas atoms in the Near-IR regime using *ab-initio* time-dependent R-matrix theory

O. Hassouneh,<sup>1,\*</sup> A.C. Brown,<sup>1</sup> and H.W. van der Hart<sup>1</sup>

<sup>1</sup>*Centre for Theoretical Atomic, Molecular and Optical Physics,  
Queen's University Belfast, Belfast BT7 1NN, UK*

(Dated:)

We demonstrate the capability of *ab-initio* time-dependent R-matrix theory to obtain accurate harmonic generation spectra of noble-gas atoms at Near-IR wavelengths between 1200 and 1800 nm and peak intensities up to  $1.8 \times 10^{14}$  W/cm<sup>2</sup>. To accommodate the excursion length of the ejected electron, we use an angular-momentum expansion up to  $L_{\max} = 279$ . The harmonic spectra show evidence of atomic structure through the presence of a Cooper minimum in harmonic generation for Kr, and of multielectron interaction through the giant resonance for Xe. The theoretical spectra agree well with those obtained experimentally.

PACS numbers: 32.80.Rm, 31.15.A-, 42.65.Ky

## I. INTRODUCTION

Advances in laser technology have provided researchers with new techniques to explore and exploit laser-matter interactions. Many experiments utilize the fundamental attosecond process—high harmonic generation (HHG)—either as the source of high energy [1] and ultrashort [2] light pulses or, more directly, as a window to attosecond dynamics [3] or detailed molecular structure [4]. These detailed spectroscopic techniques have shown that on ultrafast time-scales both multiple ionization pathways [5] and multiple-electron interference [6] are of fundamental importance in determining the dynamics.

The main influence of atomic structure on HHG can be understood through the so-called three-step model, in which a bound electron is first liberated by tunneling ionization, then driven by the laser field, before recolliding with its parent ion with the emission of a high-energy photon, all within a single cycle of the driving field [7]. The recollision step can be regarded as inverse photoionization, and therefore provides information on the basic structure of the atom, while the time-energy mapping of the recolliding electron gives a window to the attosecond-scale dynamics of the system. The highest energy of the recolliding electron—and thus, the extent of the spectrum of emitted radiation—is proportional to the square of the driving wavelength. Hence, in recent years, HHG stimulated by Near-IR (NIR) radiation (wavelengths between 1200 and 1800 nm) has gained interest. Although the total harmonic yield is significantly reduced at these higher photon energies [8, 9], the decrease in single-atom efficiency can be compensated in the macroscopic medium by ensuring good phase-matching [1].

From a measurement point-of-view, the advantage of using long-wavelength radiation is that the bandwidth of the resulting HHG spectrum leads to finer

time-resolution. Furthermore, higher laser intensities can be reached before the atom undergoes significant multiphoton ionization. As experiment continues to demonstrate the importance of multielectron effects in ultrafast processes such as HHG, it is increasingly important that there is a corresponding advance in theory, such that experimental data can be accurately interpreted and interesting dynamics can be elucidated.

To the best of our knowledge, only the time-dependent configuration-interaction singles (TDCIS) approach has been successfully applied to HHG in the NIR regime for explicitly multielectron atoms [10, 11]. In the present report, we demonstrate the capability of the R-matrix including time-dependence (RMT) approach to describe the harmonic response of general multielectron atoms in the NIR regime from first principles. The approach has two defining capabilities. Firstly, the code is optimized to run on massively parallel ( $> 1000$  cores) machines, thus making the extension to challenging physical systems more amenable. Secondly, the RMT approach can be applied to general atomic systems, including open shell atoms and ions, and can describe atomic structure induced by electron-electron repulsion in detail.

Previously, we have applied time-dependent R-matrix (TDRM) theory to investigate HHG at a wavelength of 390 nm [12–14]. These studies demonstrated that the details of the atomic structure can play a significant role in HHG. The NIR radiation regime is substantially more challenging to theory than the UV regime. For a wavelength of 1800 nm, an electron can absorb many more photons from the field, leading to a substantial increase in the angular momentum expansion. At an intensity of  $1.8 \times 10^{14}$  W/cm<sup>2</sup> at 1800 nm the excursion length of a recolliding electron can extend beyond  $200 a_0$ , so high-quality wavefunctions are required over extensive spatial regions. The implementation of time-dependent R-matrix theory in the TDRM codes slows down significantly for these large expansions, making this approach unfeasible. The RMT implementation performs much better for large angular-momentum expan-

---

\*Electronic address: ohassouneh01@qub.ac.uk

sions [15]. Hence, this approach is more suitable for the investigation of the atomic response to long-wavelength light fields.

To investigate the suitability of the RMT approach for calculations in the NIR regime, we apply the approach to HHG in Kr and Xe. These systems have been the subject of experimental investigation with the Cooper minimum in Kr studied [16] as well as the effect of the giant resonance in Xe [6]. The giant resonance has already been investigated using the TDCIS method [11], but no comparison with experimental data was made.

## II. TIME-DEPENDENT R-MATRIX THEORY

The RMT approach is the most recent implementation of time-dependent R-matrix theory [15]. This approach adopts the standard R-matrix technique of separating the physical system into two regions: an inner region, close to the nucleus, and an outer region. In the inner region, all electrons interact strongly with each other and the full Hamiltonian needs to be taken into account. In the outer region, a single ejected electron is well separated from the other electrons, and exchange effects involving this ejected electron can be neglected.

A standard R-matrix basis is used to describe the wavefunction in the inner region [17]. An  $N$ -electron atom is described as a direct product of  $(N - 1)$ -electron states of the residual ion and a complete set of single-electron functions representing the ejected electron. Additional  $N$ -electron correlation functions can be added to the basis set to improve the accuracy of the wavefunction. This is at variance with competitive methods such as TDCIS, in which the wavefunction is expressed only in terms of the Hartree-Fock ground state and singly excited configurations. At the non-relativistic Hartree-Fock level, the RMT and TDCIS methods describe the physics in the same manner, allowing for direct comparison of the methods. The TDCIS method has the capability to account for the relativistic splittings of residual ion states, giving access to spin-orbit dynamics in ultrafast processes [11]. On the other hand, the RMT approach can include the influence of double- and higher excitations in both the residual ion states, and the full system under investigation. The two methods can therefore explore the influence of a different set of interactions on the electron dynamics. Through the inclusion of correlation orbitals, the RMT approach has the capability to obtain an accurate description of the dynamics of open-shell systems as well as closed-shell systems [12, 13, 18, 19]. The capability to account for correlation in both the initial and residual ionic system is critical for this accuracy.

In the outer region, the wavefunction is described in terms of residual-ion states coupled with a finite-difference representation for the radial wavefunction of the ejected electron [15, 20]. The key distinction of RMT theory is the link between the inner and outer regions. Standard R-matrix approaches connect different regions

through the so-called R-matrix [17, 21]. In the RMT approach, the outer-region is connected to the inner region through the wavefunction itself. The outer-region grid is extended into the inner region; the inner-region wavefunction is evaluated on this grid and made available to the outer region. This suffices to propagate the outer-region wavefunction. The inner region is connected to the outer region in a traditional R-matrix fashion by determining a spatial derivative of the outer-region wavefunction at the inner-region boundary. This derivative provides the boundary information needed to update the inner-region wavefunction.

The harmonic spectrum is determined by evaluating the time-dependent expectation value of either the dipole moment or the dipole velocity [22]. In the present approach, the dipole acceleration is not suitable as we investigate Kr and Xe, for which the inner orbitals must be kept frozen. The harmonic spectra obtained through either the dipole moment or the dipole velocity show the same spectrum up to well into the cut-off regime. They differ by about 20% in overall magnitude. The main reason for this is the limited ionic basis used in the calculations.

The use of highly scalable finite-difference techniques enables efficient parallelisation of the codes beyond 1000 cores. This is key in the description of electron motion in long wavelength driving pulses, as wavepackets can be driven very far from the nucleus, necessitating a massively expanded outer region. For the investigation of HHG, however, it should be noted that details of the outgoing wavepacket are not as important when the electron is too far from the nucleus to return, especially when HHG is determined using the dipole velocity operator.

The noble-gas atoms, Kr and Xe, are described in R-matrix theory as a direct product of residual-ion states ( $\text{Kr}^+$  and  $\text{Xe}^+$ ) coupled with a complete set of outer-electron functions. In the present calculations, the residual-ion states are described using Hartree-Fock orbitals for the ground-state of  $\text{Kr}^+$  and  $\text{Xe}^+$ , respectively. We use these orbitals to generate  $4s^24p^5$  and  $4s4p^6$  residual-ion states for  $\text{Kr}^+$ , and  $4d^{-1}$ ,  $5s^{-1}$  and  $5p^{-1}$  initial states for  $\text{Xe}^+$ . To investigate the influence of the various shells on HHG in Xe, we have carried out additional calculations in which the  $4d^{-1}$  residual-ion state is included or excluded. We have also performed calculations including the  $4p^{-1}$  state and find that its inclusion does not affect the HHG spectra.

## III. CALCULATION PARAMETERS

The description of Kr and Xe includes all available channels up to a maximum total angular momentum  $L_{\text{max}} = 180$  for Kr and 279 for Xe. The spectra were tested for convergence with respect to angular momentum. The time-step in the wave function propagation for this calculation is normally set to 0.24 as. Additional calculations were carried out at a shorter time-step of 0.12

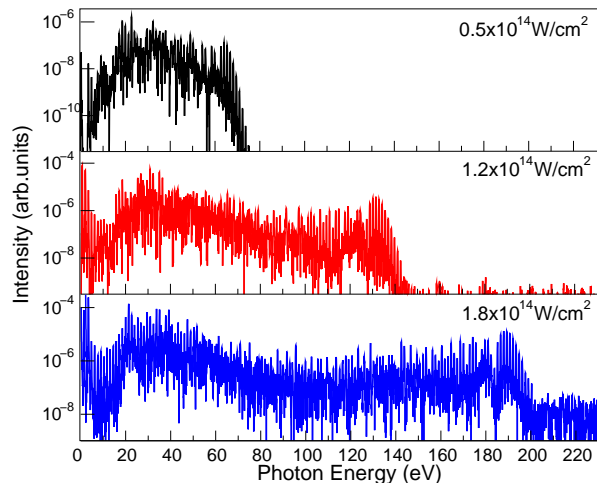


FIG. 1: (Color Online) Calculated harmonic spectra of Kr at a wavelength of 1800 nm for different peak laser intensities.

as, with no significant change in the spectra. The pulse profile is given by a four-cycle  $\sin^2$  turn-on followed by two cycles at peak pulse intensity and a four-cycle  $\sin^2$  turn-off (4-2-4). To investigate the harmonic spectrum for short pulses, additional spectra were obtained for a pulse with a two-cycle  $\sin^2$  turn-on followed immediately by a two-cycle  $\sin^2$  turn-off (2-0-2).

The R-matrix inner region has a radius of  $20 a_0$ . The continuum functions are described using a set of 60 B-splines of order  $k = 9$ , for each available angular momentum of the outgoing electron. In the outer region we set the outer boundary to about  $5000 a_0$  to reduce unphysical reflections of the wave function from this boundary. Re-scattered electrons can have an energy of  $10 U_p$ , with  $U_p$  the ponderomotive potential [23]. This energy is about 550 eV in the present calculations. Hence, large box sizes are required. The calculations were performed on ARCHER, the UK's supercomputing facility, and typically employed around 1500 cores for 8 hours.

#### IV. RESULTS

The main outcomes of the calculations are the time-dependent expectation values of the dipole operator and the dipole velocity operator. These time-dependent expectation values are Fourier transformed and squared to obtain the harmonic spectrum. Figure 1 shows the harmonic spectrum obtained for Kr irradiated by a 4-2-4 laser pulse, with a total duration of 60 fs, at a wavelength of 1800 nm as a function of peak intensity. The spectra show the standard form of odd harmonics of the fundamental photon energy with a well-defined plateau region and a cut-off energy of 70 eV at  $0.5 \times 10^{14} \text{ W/cm}^2$  increasing to 188 eV at  $1.8 \times 10^{14} \text{ W/cm}^2$ . This is in line with the cut-off formula:  $E_c = 1.3I_p + 3.17U_p$ , where  $I_p$  is the ionization potential and  $U_p$  the ponderomotive po-

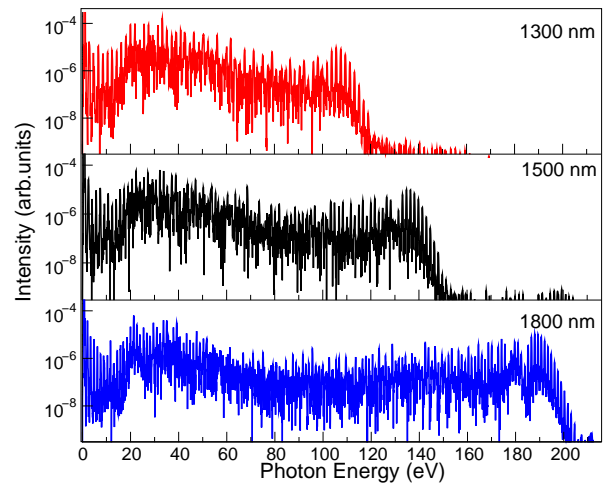


FIG. 2: (Color online) Calculated harmonic spectrum of Kr at a peak intensity of  $1.8 \times 10^{14} \text{ W/cm}^2$  for different laser wavelengths.

tential [24].

At the highest peak intensity of  $1.8 \times 10^{14} \text{ W/cm}^2$ , Fig. 1 shows a clear influence of atomic structure on the harmonic spectrum through a minimum in the harmonic yield at a photon energy of around 85 eV. This minimum is also visible at a peak intensity of  $1.2 \times 10^{14} \text{ W/cm}^2$ , but at  $0.5 \times 10^{14} \text{ W/cm}^2$ , the harmonic plateau does not extend sufficiently far. This is a so-called Cooper minimum, in which the radial dipole matrix element between the  $4p$  orbital in Kr and the continuum  $d$  orbital vanishes. The photorecombination step in the three-step model is the reverse process of photoionization, and it will thus be affected similarly: when the radial matrix element vanishes, photorecombination is not allowed. This minimum has been observed in photoionization spectra and occurs at a photon energy around 84 eV [25], in line with the present observations.

Figure 2 shows the dependence of the harmonic cut-off on laser wavelength for Kr. We observe a cut-off energy of 115 eV at 1300 nm, 140 eV at 1500 nm and 188 eV at 1800 nm, in line with the cut-off formula [24]. The position of the minimum in the harmonic yields is largely independent of driving wavelength. At the shortest wavelength, the spectrum barely extends to the energy of the Cooper minimum. Unambiguous observation of the minimum is only possible at the longer wavelengths.

Figure 3 shows a comparison with the experimental HHG spectrum [16]. Although the theoretical spectrum extends up to 190 eV, the experimental spectrum was presented only for photon energies up to 150 eV. Figure 3 shows excellent agreement between the two spectra, demonstrating that RMT theory has the capability to predict harmonic spectra in the NIR regime. We note, however, that while RMT calculates single-atom HHG spectra, the experimental spectra include propagation effects, which may indicate a preference for either the so-called short or long trajectories [26].

Figure 3 suggests the minimum appears between 90-100 eV in experiment, whereas the calculated minimum appears closer to 85 eV. However, the position of the theoretical minimum is difficult to assign unambiguously, as there is variation in intensity between neighbouring harmonics. Furthermore, the presented experimental data is an averaged spectrum, and the different rates of increase around the minimum may have shifted the experimentally observed minimum to higher energy.

The comparison between experiment and theory is more difficult for harmonic photons with an energy greater than 150 eV. One of the reasons for this difficulty is the experimental pulse length. In Fig. 4, we compare the harmonic spectrum obtained for our current 4-2-4 pulse with a pulse consisting of a 2-cycle  $\sin^2$  turn-on, followed by a 2-cycle  $\sin^2$  turn-off. For both profiles, the carrier-envelope phase is set to  $0^\circ$ . The full-width at half-maximum of the 2-0-2 pulse is about 8.7 fs, which is comparable with the 10 fs pulse used in the experiment. This reduction in pulse length has a significant effect on the harmonic spectrum. Classical calculations show that only one electron trajectory leads to recollisions with energies greater than 140 eV. This leads to a broad spectrum as peaks separated by twice the fundamental photon energy require interference between multiple trajectories.

We have investigated the influence of the multielectron interaction on HHG in Xe for a 4-cycle,  $1.9 \times 10^{14} \text{ W/cm}^2$ , 1800 nm pulse. The photoionization spectrum of Xe is dominated by the so-called giant resonance, in which a  $4d$  electron is excited into a short-lived quasi-bound resonance of  $f$  character [27]. However, this resonance cannot be thought of as a single-electron effect: partial photoionization spectra demonstrate evidence of the resonance in the photoemission of the  $5s$  and the  $5p$  electron, as well as photoemission of the  $4d$  electron.

The most likely electron to be removed from the Xe

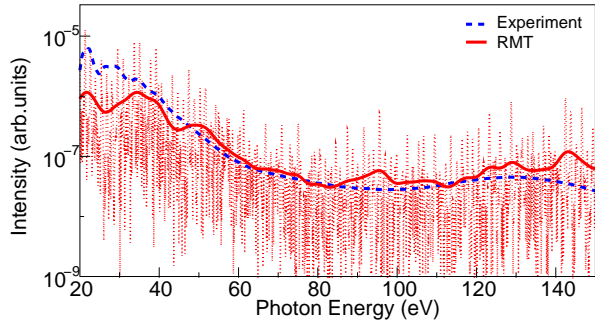


FIG. 3: (Color Online) HHG spectrum for Kr calculated using RMT (dotted, red line), smoothed spectrum (solid, red line) and the experimental spectrum (dashed, blue line, [6]) at a wavelength of 1800 nm and a peak intensity of  $1.8 \times 10^{14} \text{ W/cm}^2$ . Although the theoretical spectrum extends to 190 eV, the experimental spectrum was only reported for photon energies up to 150 eV. The experimental data has been renormalised for comparison with the theoretical spectrum.

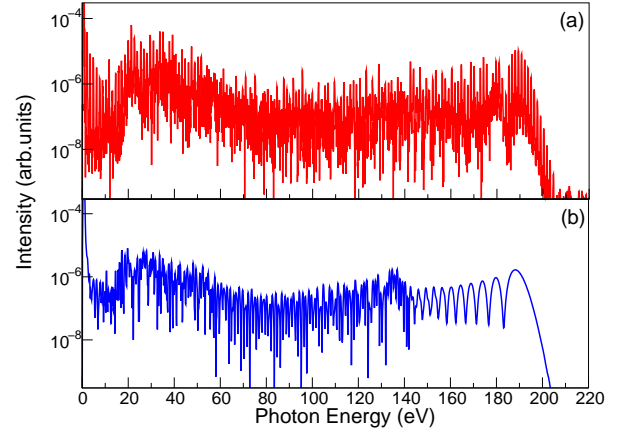


FIG. 4: (Color Online) The HHG spectrum of Kr at a wavelength of 1800 nm and a peak intensity of  $1.8 \times 10^{14} \text{ W/cm}^2$  for a 10-cycle pulse with a 4-2-4 profile (a) and a 4-cycle pulse with a 2-0-2 profile (b).

atom in the ionization step of the recollision model is the outermost  $5p$  electron, particularly at long wavelengths. The observation of the giant resonance is then a clear indication of electron-electron interactions: a  $4d$  electron interacts with the recolliding electron to be promoted into the  $5p$  hole. This allows the recolliding electron to recombine into the  $4d$  shell— for which the photorecombination matrix elements are particularly large relative to the  $5p$  matrix elements— leading to a broad resonance in the HHG yield. To demonstrate this latter point, calculations have been carried out which either allow or disallow emission of one of the  $4d$  electrons.

Figure 5 shows the calculated harmonic spectrum for Xe irradiated by 1800 nm laser light with a peak intensity of  $1.9 \times 10^{14} \text{ W/cm}^2$ . The figure compares the harmonic spectrum obtained both by including and neglecting the influence of the  $4d$  electron. In line with

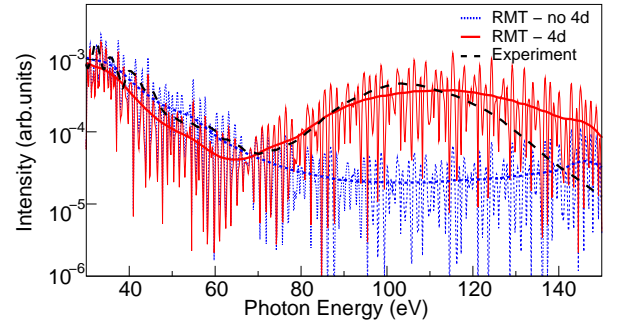


FIG. 5: (Color online) The harmonic spectrum for Xe irradiated by an 11 fs, 1800 nm laser pulse with a peak intensity of  $1.9 \times 10^{14} \text{ W/cm}^2$  as obtained in experiment (dashed, black line, [6]) and using the present approach, either including emission of a  $4d$  electron (solid, red line) or excluding this emission (dotted, blue line). The thick lines indicate the smoothed theoretical results. The experimental data has been renormalised for comparison with the theoretical spectra.

TDCIS calculations [10], opening the  $4d$  shell increases the harmonic yield by about an order of magnitude in the neighbourhood of the giant resonance at around 115 eV. The calculated spectrum shows good agreement with experiment [6] up to a photon energy of about 100 eV, when the experimental harmonic yield drops off faster than the theoretical ones. Thus the theoretical resonance appears to be broader than the experimental resonance which is centered on 100 eV. Again, these differences may be due to macroscopic propagation effects. However, the description of the resonance might also be improved by including more electron-correlation effects, to describe changes in the  $4d$  and  $5p$  orbitals during HHG. Although it is, in principle, possible to include additional orbitals to account for these changes, their inclusion would significantly increase the number of residual-ion states to account for, rendering the calculations unfeasible at present.

## V. CONCLUSIONS

In conclusion, we have demonstrated the feasibility to investigate HHG in general atomic systems in the NIR regime from first principles with full inclusion of electron-electron repulsion. Specifically, we have applied the RMT codes to investigate HHG in Kr and Xe at wavelengths up to 1800 nm. Experimental spectra show a significant influence of atomic structure, which is well reproduced in

the theoretical calculations. The present investigations only concern noble-gas atoms, as these are the systems of main experimental interest. However, the RMT approach has already been applied to photoionization of atomic systems with open outer shells, such as  $\text{Ne}^+$  and C [18, 19]. The approach should therefore be capable of obtaining HHG spectra for general atomic systems in the NIR regime.

HHG is only one of the many aspects of laser-matter interactions that has been investigated experimentally. For example, experiment has also investigated ejected-electron momentum distributions for atoms and ions irradiated by short 1800 nm fields. The theoretical description of these distributions is significantly more sensitive to the number of total angular momenta included in the calculations. It will therefore be interesting to explore whether other aspects of laser-matter interactions at 1800 nm can also be investigated accurately using the RMT approach.

The authors thank David Villeneuve and Andrew Shiner for providing the experimental data in numerical form, and Stefan Pabst for additional, theoretical data. OH acknowledges financial support from the University of Jordan. HWH acknowledges financial support from the UK EPSRC under grant no. EP/G055416/1 and the EU Initial Training Network CORINF. This work used the ARCHER UK National Supercomputing Service (<http://www.archer.ac.uk>).

- 
- [1] T. Popmintchev *et al.*, Science **336**, 1287 (2012).
  - [2] P. M. Paul, E. S. Toma, P. Breger, G. Mullot, F. Augé, P. Balcou, H. G. Muller, and P. Agostini, Science **292**, 1689 (2001).
  - [3] S. Baker, J. S. Robinson, C. A. Haworth, H. Teng, R. A. Smith, C. C. Chirilă, M. Lein, J. W. G. Tisch, and J. P. Marangos, Science **312**, 424 (2006).
  - [4] J. Itatani, J. Levesque, D. Zeidler, H. Niikura, H. Pépin, J. C. Kieffer, P. B. Corkum, and D. M. Villeneuve, Nature **432**, 867 (2004).
  - [5] O. Smirnova, Y. Mairesse, S. Patchkovskii, N. Dudovich, D. Villeneuve, P. B. Corkum, and M. Y. Ivanov, Nature **460**, 972 (2009).
  - [6] A. D. Shiner, B. E. Schmidt, C. Trallero-Herrero, H. J. Wörner, S. Patchkovskii, P. B. Corkum, J.-C. Kieffer, F. Légaré, and D. M. Villeneuve, Nat. Phys. **7**, 464 (2011).
  - [7] P. B. Corkum, Phys. Rev. Lett. **71**, 1994 (1993).
  - [8] J. Tate, T. Augustine, H. G. Muller, P. Salieres, P. Agostini, and L. F. DiMauro, Phys. Rev. Lett. **98**, 013901 (2007).
  - [9] A. D. Shiner, C. Trallero-Herrero, N. Kajumba, H.-C. Bandulet, D. Comtois, F. Légaré, M. Giguère, J.-C. Kieffer, P. B. Corkum, and D. M. Villeneuve, Phys. Rev. Lett. **103**, 073902 (2009).
  - [10] S. Pabst and R. Santra, Phys. Rev. Lett. **111**, 233005 (2013).
  - [11] S. Pabst and R. Santra, J. Phys. B: At. Mol. Opt. Phys. **47**, 124026 (2014).
  - [12] A. C. Brown and H. W. van der Hart, Phys. Rev. A **86**, 063416 (2012).
  - [13] A. C. Brown and H. W. van der Hart, Phys. Rev. A **88**, 033419 (2013).
  - [14] O. Hassouneh, A. C. Brown, and H. W. van der Hart, Phys. Rev. A **89**, 033409 (2014).
  - [15] L. R. Moore, M. A. Lysaght, L. A. A. Nikolopoulos, J. S. Parker, H. W. van der Hart, and K. T. Taylor, J. Mod. Optics **58**, 1132 (2011).
  - [16] A. D. Shiner, B. E. Schmidt, C. Trallero-Herrero, P. B. Corkum, J.-C. Kieffer, F. Légaré, and D. M. Villeneuve, Journal of Physics B: Atomic, Molecular and Optical Physics **45**, 074010 (2012).
  - [17] P. G. Burke, *R-Matrix Theory of Atomic Collisions* (Springer Verlag, Heidelberg, 2011).
  - [18] H. W. van der Hart and R. Morgan, Phys. Rev. A **90**, 013424 (2014).
  - [19] H. F. Rey and H. W. van der Hart, Phys. Rev. A **90**, 033402 (2014).
  - [20] M. Lysaght, L. Moore, L. Nikolopoulos, J. Parker, H. van der Hart, and K. Taylor, in *Quantum Dynamic Imaging*, edited by A. D. Bandrauk and M. Ivanov (Springer New York, 2011), CRM Series in Mathematical Physics, pp. 107–134, ISBN 978-1-4419-9490-5.
  - [21] M. A. Lysaght, H. W. van der Hart, and P. G. Burke, Phys. Rev. A **79**, 053411 (2009).
  - [22] A. C. Brown, D. J. Robinson, and H. W. van der Hart,

- Phys. Rev. A **86**, 053420 (2012).
- [23] W. Becker, F. Grasbon, R. Kopold, D. B. Milošević, G. G. Paulus, and H. Walther (Academic Press, 2002), vol. 48 of *Advances In Atomic, Molecular, and Optical Physics*, pp. 35 – 98.
  - [24] M. Lewenstein, P. Balcou, M. Y. Ivanov, A. L’Huillier, and P. B. Corkum, Phys. Rev. A. **49**, 2117 (1994).
  - [25] J. Samson and W. Stolte, J. Elec. Spec. Rel. Phenom. **123**, 265 (2002).
  - [26] O. Smirnova and M. Y. Ivanov, in *Attosecond and XUV Physics*, edited by T. Shultz and M. Vrakking (Wiley VCH, 2013).
  - [27] U. Becker, D. Szostak, H. G. Kerkhoff, M. Kupsch, B. Langer, R. Wehlitz, A. Yagishita, and T. Hayaishi, Phys. Rev. A **39**, 3902 (1989).